Kinetics and Energetics of the Binding between Barley α-Amylase/Subtilisin Inhibitor and Barley α-Amylase 2 Analyzed by Surface Plasmon Resonance and Isothermal Titration Calorimetry†

Peter K. Nielsen,‡ Birgit C. Bønsager,‡ Carolyn R. Berland,‡ Bent W. Sigurskjold,§ and Birte Svensson*,‡

Carlsberg Laboratory, Department of Chemistry, Gamle Carlsberg Vej 10, DK-2500 Copenhagen Valby, Denmark, and Department of Biochemistry, August Krogh Institute, University of Copenhagen, Universitetsparken 13, DK-2100 Copenhagen Ø, Denmark

Received August 2, 2002

ABSTRACT: The kinetics and energetics of the binding between barley α-amylase/subtilisin inhibitor (BASI) or BASI mutants and barley α-amylase 2 (AMY2) were determined using surface plasmon resonance and isothermal titration calorimetry (ITC). Binding kinetics were in accordance with a 1:1 binding model. At pH 5.5, $[Ca^{2+}] = 5$ mM, and 25 °C, the k_{on} and k_{off} values were $8.3 \times 10^{+4}$ M^{-1} s^{-1} and 26.0×10^{-4} s^{-1}, respectively, corresponding to a K_D of 31 nM. K_D was dependent on pH, and while k_{off} decreased 16-fold upon increasing pH from 5.5 to 8.0, k_{on} was barely affected. The crystal structure of AMY2−BASI shows a fully hydrated Ca^{2+} at the protein interface, and at pH 6.5 increase of $[Ca^{2+}]$ in the 2 μM to 5 mM range raised the affinity 30-fold mainly due to reduced k_{off}. The K_D was weakly temperature-dependent in the interval from 5 to 35 °C as k_{on} and k_{off} were only increasing 4- and 12-fold, respectively. A small salt dependence of k_{on} and k_{off} suggested a minor role for global electrostatic forces in the binding and dissociation steps. Substitution of a positively charged side chain in the mutant K140L within the AMY2 inhibitory site of BASI accordingly did not change k_{on}, whereas k_{off} increased 13-fold. ITC showed that the formation of the AMY2−BASI complex is characterized by a large exothermic heat ($\Delta H = -69 \pm 7$ kJ mol^{-1}), a K_D of 25 nM (27 °C, pH 5.5), and an unfavorable change in entropy ($-T\Delta S = 26 \pm 7$ kJ mol^{-1}). Calculations based on the thermodynamic data indicated minimal structural changes during complex formation.

Barley α-amylase/subtilisin inhibitor (BASI)[1] is an endogenous inhibitor of the high p*I* isozyme α-amylase 2 (AMY2) but does not inhibit the low p*I* isozyme α-amylase 1 (AMY1) (*1*−*3*), which has 80% sequence identity with AMY2 (*4*−*6*). BASI moreover inhibits serine proteases of the subtilisin family (*1*). BASI shares high sequence identity with cereal inhibitors, WASI from wheat (*7*, *8*) and RASI from rice (*9*). These double-headed inhibitors belong to the Kunitz-type trypsin inhibitor family of β-trefoil fold proteins that includes the more distantly related interleukin 1-α and 1-β (*10*, *11*) and fibroblast growth factors (*12*). The precise function of BASI in the seed remains unclear, but it has been suggested that it plays a role in control of AMY2 activity during premature sprouting and in plant defense acting on serine proteases of pathogens and pests (*1*−*3*).

Recently, the crystal structure of the complex between AMY2 and BASI has been solved at 1.9 Å resolution (*13*). The complex was shown to be very stable with K_i determined to 0.07 and 0.22 nM by stopped-flow fluorescence spectroscopy (*14*) and AMY2 activity inhibition assay, respectively (*2*). A structural analysis of the AMY2−BASI complex interface describes at least 48 residues from the two proteins to be in contact in the complex (*13*). Seventeen of these are in direct hydrogen bond contact while eight participate in water-mediated hydrogen bonds. The binding surface is about 2355 $Å^2$ and comprises interactions within the B-domain and the active site of AMY2 (*13*). BASI does not, however, bind directly to the three catalytic carboxyl groups in AMY2, but a unique, completely hydrated Ca^{2+} that via water molecules in a network connects the three catalytic acids of AMY2 with side chains in BASI is located in the crystal structure of the protein interface (Figure 1). This Ca^{2+} is only found in the AMY2−BASI complex and has not been reported in the crystal structure of AMY2 (*15*, *16*). The structure of a complex with subtilisin remains to be determined, but a low-resolution structure between WASI and proteinase K has indicated an important role in inhibition of a loop located at a site opposite to the α-amylase binding site in the inhibitor (*17*).

The protein−protein interaction between AMY2 and BASI is unique among the currently known types of α-amylase

† This work is supported by a grant from the EU Framework V Programme (QLK1-2000-00811) to the project GEMINI. B.C.B. was supported by a Novo Scholarship.

* To whom correspondence should be addressed. Phone: +45 33 27 53 45. Fax: +45 33 27 47 08. E-mail: bis@crc.dk.

‡ Gamle Carlsberg Vej 10.

§ University of Copenhagen.

[1] Abbreviations: AMY1 and AMY2, barley α-amylase 1 and 2, respectively; ASA, accessible surface area; BASI, barley α-amylase/subtilisin inhibitor; ITC, isothermal titration calorimetry; rBASI, recombinant barley α-amylase/subtilisin inhibitor; RU, resonance units; SPR, surface plasmon resonance.

10.1021/bi020508+ CCC: $25.00
Published on Web 01/22/2003

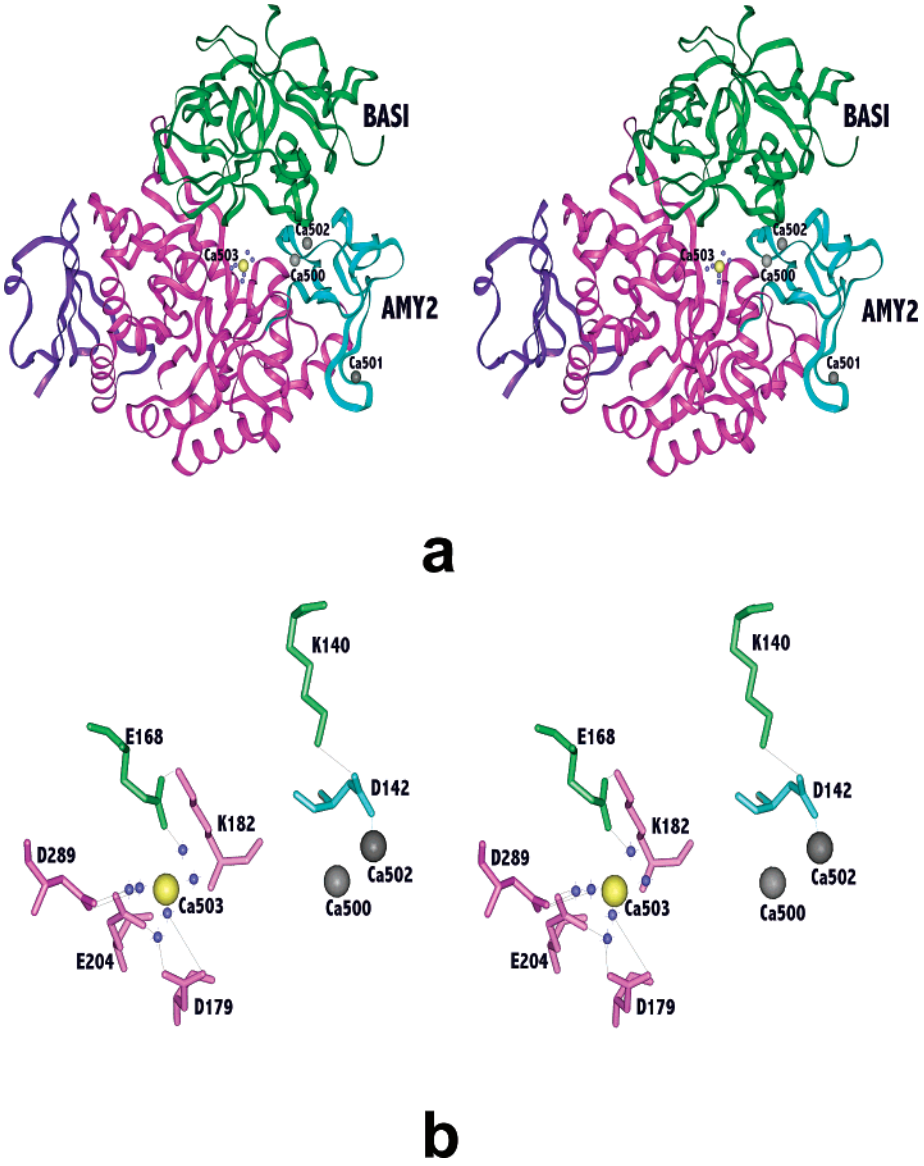

FIGURE 1: Molecular structure of the AMY2−BASI complex (*13*). (a) Global view stereo drawing of the complex highlighting the fully hydrated Ca^{2+} (yellow) at the protein−protein interface and the three structural Ca^{2+} in AMY2 (gray). The Ca^{2+}-coordinated water molecules are shown in blue. AMY2 contains domain A (purple), domain B (light blue), and domain C (dark purple). BASI is in green. (b) Close-up stereo drawing of the fully hydrated Ca^{2+} at the AMY2−BASI interface. The catalytic acids and Lys182 in AMY2 are in purple and Asp142 within domain B is in light blue. Lys140 and Glu168 in BASI are in green. Associated hydrogen bonds are shown as gray dashed lines.

protein inhibitor complexes for which the structures have been solved: porcine pancreatic α-amylase and Tendamistat (*18*), porcine pancreatic α-amylase and α-AI, a lectin-like bean inhibitor (*19*), yellow meal worm α-amylase and a bifunctional inhibitor from *Ragi* (Indian finger millet) (*20*), and the same enzyme with an inhibitor from *Amaranth* (*21*). In three cases the catalytic acids in the enzyme and the inhibitor directly interact, i.e., the two of porcine pancreas α-amylase and the yellow meal worm α-amylase *Ragi* inhibitor complex (*18*−*20*). The inhibitor from *Amaranth* in contrast has contact through a water molecule (*21*). Interestingly, only αAI and the *Amaranth* inhibitor are described to exert substrate mimicry (for review on α-amylase plant inhibitors, see ref *22*).

To achieve thorough understanding of the binding, a biophysical description of the role of the hydrated calcium and other factors in the stabilization of the complex is required to complement the model provided by the crystal structure of the AMY2−BASI complex. Thus through a series of surface plasmon resonance (SPR) and isothermal titration calorimetry (ITC) experiments, the kinetics and the thermodynamics of the binding between AMY2 and BASI were analyzed at different temperatures, pH, ionic strengths, and [Ca^{2+}]. The study allowed direct comparison between two biophysical techniques and is the first demonstration of Ca^{2+}-modulated kinetics of the interaction between BASI and AMY2 with relevance therefore for related systems of proteinaceous inhibitors and protein−protein interactions.

EXPERIMENTAL PROCEDURES

Proteins. AMY2 (the AMY2-2 form was used in this work) and AMY1 were purified from kilned and green barley malt (cvs. Triumph or Menuet), respectively, while BASI was purified from mature barley (cv. Piggy) seeds (*2*, *6*, *23*). Savinase was a kind gift of Dr. Steen Bech Sørensen,

Carlsberg Research Laboratory. The protein concentrations were determined by amino acid analysis or by spectrophotometric methods using $\epsilon_{280} = 24 \times 10^3\ M^{-1}\ cm^{-1}$ for AMY2 (*24*), $13 \times 10^3\ M^{-1}\ cm^{-1}$ for BASI (*25*), and $23 \times 10^3\ M^{-1}\ cm^{-1}$ for savinase (*26*). Recombinant wild-type BASI (rBASI) and the BASI mutants, K140L and E168Q, were produced using an *Escherichia coli* expression system. BASI cDNA (*27*) was amplified by PCR using primers (DNA technologies, Århus, Denmark) containing *Nde*I and *Sap*I restriction sites (in bold) in the 5′ and 3′ ends, respectively: 5′ **CATATG**GCCGATCCGCCGCCGGTGCACG 3′ and 5′ **GCTCTTC**CGCAAGCGGGCGGCGCCTTCTTGAACA 3′. For E168Q rBASI a 5′ primer containing a mutated site was synthesized: 5′ **GCTCTTC**CGCAAGCGGGCGGCGCCTTCTTGAACACGACGACATGGTATGGCTGGGTGG 3′ (underlining indicates the mutated codon). For K140L rBASI a mutational primer 5′ CACGACATCAGCAGGTACTCGTGC 3′ was used for generation of a megaprimer before the cDNA was amplified. The wild-type and mutated BASI sequences were cloned into a pTYB1 expression vector (New England Biolabs, Beverly, MA) that encodes an intein tag in conjugation with a chitin binding domain (Intein-CBD) adjacent to the C-terminus of BASI. The intein carries out a self-cleavage reaction to release the target protein (*28*). The recombinant fusion proteins were produced essentially as described by the manufacture in *E. coli* BL21(DE3) cells (Stratagene, Amsterdam, The Netherlands) grown overnight at 20 °C. The cells were resuspended in 20 mM Hepes, pH 8.0, 0.5 M NaCl, and 0.1 mM EDTA and disrupted using a French press (American Instrument Co., Baltimore, MD). After centrifugation the supernatant was applied to a chitin bead affinity column (New England Biolabs), and the column was washed with 20 mM Hepes, pH 8.0, 0.05 M NaCl, and 0.1 mM EDTA and then flushed with the same buffer plus 30 mM DTT. The flow was stopped, and rBASI was eluted after 24 h at 4 °C (*28*). Fractions containing rBASI were combined and gel filtered on a Superose 12 HR 10/30 column (Amersham Biosciences, Uppsala, Sweden) equilibrated with 20 mM Tris-HCl, pH 8.0, and 0.15 M NaCl using an ÄKTA explorer automatic chromatograph. rBASI was >98% pure as estimated by SDS−PAGE and isoelectric focusing (Novex gels, Invitrogen, Groningen, The Netherlands). rBASI concentrations were determined by amino acid analysis on a Biochrom 20 analyzer (Pharmacia, Uppsala, Sweden).

Biotinylation of AMY2. AMY2 in 10 mM Mes, pH 6.7, and 5 mM $CaCl_2$ (7.0 mg $\times mL^{-1}$) was biotinylated through covalent coupling of primary amino groups with EZ-Link sulfo-NHS-LC-biotin [sulfosuccinimidyl-6-(biotinamido)hexanoate] (Pierce, Rockford, IL) at a 1:10 molar ratio for 30 min at room temperature. Biotinylated AMY2 was separated from the remaining reagent on a PD-10 desalting column (Amersham Pharmacia Biotechnology, Uppsala, Sweden) equilibrated in 10 mM Hepes, pH 7.4, 150 mM NaCl, and 5 mM $CaCl_2$. The activity of the biotinylated AMY2 preparation was measured using 6.25 mg $\times mL^{-1}$ insoluble Blue Starch (customer preparation, Pharmacia) as substrate in 20 mM sodium acetate, pH 5.5, containing 5 mM $CaCl_2$ and 0.05% BSA (total volume of 4 mL). After incubation for 15 min at 37 °C the reaction was stopped by adding 0.5 M NaOH (1 mL). Aliquots (1 mL) were centrifuged, and the supernatants (300 μL) were transferred to a microtiter plate for A_{620} reading (Ceres UV900 HDI microplate reader, Biotek Instruments, Inc.) (*29*). One unit corresponded to the amount of enzyme giving a ΔA_{620} of 0.001 in 15 min in the final volume (5 mL). The specific activity was essentially unchanged by the biotinylation.

Surface Plasmon Resonance. The kinetics of the binding between BASI from seeds, rBASI wild-type and mutants, and AMY2 or savinase was analyzed in real time by SPR using a BIAcore 3000 (BIAcore, Uppsala, Sweden) (*30*−*32*). Streptavidin−biotin coupling of AMY2 was achieved by injection of randomly biotinylated AMY2 (10 $\mu g \times mL^{-1}$) in running buffer [10 mM Hepes, pH 7.4, 150 mM NaCl, 5 mM $CaCl_2$, 0.005% (v/v) surfactant P20] on a streptavidin-coated sensor chip (Sensor Chip SA, BIAcore) at a flow rate of 10 $\mu L \times min^{-1}$ for 4 min. Random amine coupling of BASI and savinase was carried out by injecting proteins (2 $\mu g \times mL^{-1}$ each) in 10 mM sodium acetate, pH 5.0, following preactivation of the carboxymethylated dextran matrix (CM5 sensor chip) using *N*-hydroxysuccinimide/*N*-ethyl-*N*′-[3-(diethylamino)propyl]carbodiimide.

BIAcore 3000 sensorgrams [resonance units (RU) versus time] were recorded at a flow rate of 30 $\mu L \times min^{-1}$ at 25 °C, using five concentrations (20−300 nM) of analytes in running buffer. The analyses were performed in duplicate using sensor chips coupled with 300−1000 RU of protein. The association and dissociation data were collected for 4 and 15 min, respectively. The AMY2 and BASI sensor chips were regenerated at the end of each run by two injections of 30 μL of 10 mM sodium acetate, pH 5.0, while regeneration of the savinase chips was achieved by extending the dissociation phase by 5 min. Data obtained from parallel flow cells without coupled ligands (derivatized in the presence of buffer only) served as blank sensorgrams for subtraction of changes in the bulk refractive index. The AMY2−BASI interaction was analyzed at five temperatures, ranging from 5 to 40 °C. As signal detection is sensitive to temperature variations, the detector was reset at each new temperature using the "normalize" command. In the [Ca^{2+}] dependence analysis the residue concentration (2−6 μM) of Ca^{2+} was estimated from the dilution of the AMY2 stock solution buffer (10 mM Mes, pH 6.7, 5 mM $CaCl_2$), which was made up in MilliQ water. The AMY2−BASI complex for interaction analysis with savinase was prepared by incubation at a 1:1 molar ratio for at least 30 min in running buffer at room temperature before injection.

The sensorgrams were analyzed using BIAevaluation version 3.1 software that provides both numerical integration and global fitting algorithms. The data were fitted to a single-site interaction model [1:1 (Langmuir) binding: $A + B \rightleftharpoons AB$]. Assuming pseudo-first-order interaction kinetics, the rate of complex formation during sample injection is given by $d[AB]/dt = k_{on}[A][B] - k_{off}[AB]$, which may be expressed as $dR/dt = k_{on}CR_{max} - (k_{on}C + k_{off})R$, where dR/dt is the rate of change of the SPR signal, C is the concentration of analyte, R_{max} is the maximum analyte binding capacity in RU, and R is the recorded SPR signal in RU at time t. k_{off} values were determined from the data collected during the dissociation phase ($dR/dt = -k_{off}R$), while k_{on} values were derived from the above rate equation for complex formation. The equilibrium dissociation constant was calculated from the kinetic rate constants ($K_D = k_{off}/k_{on}$). Details of the rate equations are described in the BIAevaluation version 3 software manuals and ref *33*. $\Delta\Delta G = \Delta G_{mutant} - \Delta G_{wild\ type}$

was calculated as $RT \ln(K_{D(mut)}/K_{D(wt)})$, where R is the gas constant ($R = 8.314$ J× mol^{-1}× K^{-1}) and $T = 298.15$ K.

Isothermal Titration Calorimetry. Calorimetric measurements of the AMY2−BASI interaction were performed on a MicroCal OMEGA titration microcalorimeter (MicroCal Inc., Northhamptom, MA) (*34*). Protein solutions were dialyzed against either 40 mM Hepes, pH 6.8, 5 mM $CaCl_2$, and 0.2 M NaCl or 40 mM sodium acetate, pH 5.5, and 5 mM $CaCl_2$, passed through a 0.2 μm filter, and degassed by stirring under vacuum before use. Experiments were performed at 11 ± 0.2, 25 ± 0.2, 37 ± 0.2, 46 ± 0.2, and 55 ± 0.2 °C at pH 6.8 and pH 5.5 at 27 ± 0.2 °C. The sample cell was filled with AMY2 solution (28 μM), and while being stirred at 400 rpm, the system was allowed to equilibrate to an rms noise value of 0.008 μJ ×s^{-1} before the start of titration. The injection syringe was filled with BASI solution (282 μM), and repeated injections were made. Injections were continued beyond saturation of AMY2 to allow for determination of heat of dilution. The calorimeter was calibrated using standard electrical pulses generated using the provided software. Calorimetric data were analyzed by integration of resultant peaks (ORIGIN software; MicroCal Software, Inc.). Nonlinear regression fitting to the isotherm gave the equilibrium association constant of the ligand, K_A, the molar heat of binding, $\Delta H°$, the concentration of binding sites (stoichiometry), and the heat of dilution of the proteins. Using these parameters the free energy and the entropy were calculated using standard thermodynamics relationships: $\Delta G° = -RT \ln K_A = \Delta H° - T\Delta S°$.

The changes in accessible surface area of apolar (ΔASA_{ap}) and polar (ΔASA_{pol}) groups in AMY2 and BASI upon binding were calculated from the empirical relationships to heat capacity (ΔC_p) and enthalpy ($\Delta H°$) changes as follows: $\Delta C_p = -1.88\Delta ASA_{ap} + 1.09\Delta ASA_{pol}$; $\Delta H^{60} = 39.3\Delta ASA_{ap} - 131\Delta ASA_{pol}$, where ΔH^{60} is the binding enthalpy at 60 °C (*35*). The heat capacity change for the complex formation, ΔC_p, was determined as the slope from a linear plot of $\Delta H°$ versus T ($\Delta C_p = \delta\Delta H°/\delta T$), and the enthalpy at 60 °C (ΔH^{60}) was extrapolated from the same plot.

Molecular Graphics. The structure of the AMY2−BASI complex (*13*) was obtained from the Protein Data Bank (*36*), accession number 1AVA, and the figures were made using the software program Insight II (97.0), Molecular Simulations Inc., San Diego, CA.

RESULTS

Preparation and Specificity of BASI, AMY2, and Savinase Sensor Chips. BASI and savinase were immobilized on a carboxymethylated dextran matrix on a BIAcore CM5 sensor chip by random amine coupling. However, because this immobilization of AMY2 resulted in loss of BASI binding ability, biotinylated AMY2 was subsequently immobilized on a streptavidin-coated BIAcore SA sensor chip. To minimize mass transport effects, low-loaded surfaces, about 300 RU, and high flow rates, 30 μL ×min^{-1}, were used in the binding measurements. AMY2 binding to immobilized BASI was specific as no binding occurred to the control flow cell. Passing a high concentration of BASI (2 μM) over the AMY2 surface, at three flow rates, 5, 15, and 75 μL ×min^{-1}, resulted in similar apparent k_{on} values of 2.9×10^4, 2.2×10^4, and 2.8×10^4 M^{-1} s^{-1}, respectively, suggesting the absence of an adverse mass transport effect.

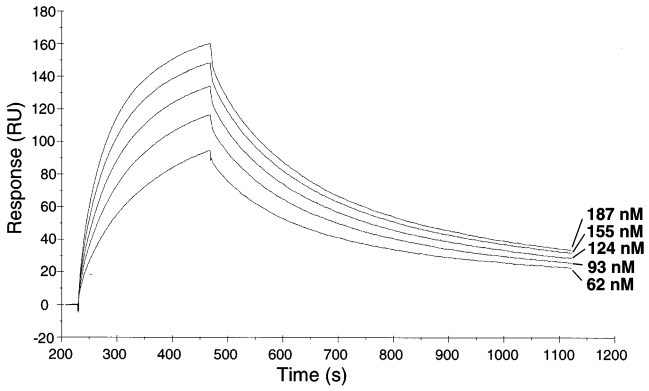

FIGURE 2: Representative real-time binding sensorgrams for the AMY2−BASI interaction measured by SPR. AMY2 of varying concentrations (62, 93, 124, 155, and 187 nM) was injected over immobilized BASI as shown by the sensorgrams. The measurements were carried out in 10 mM Mes, 150 mM NaCl, pH 5.5, 0.005% P-20, and 5 mM $CaCl_2$ at 25 °C.

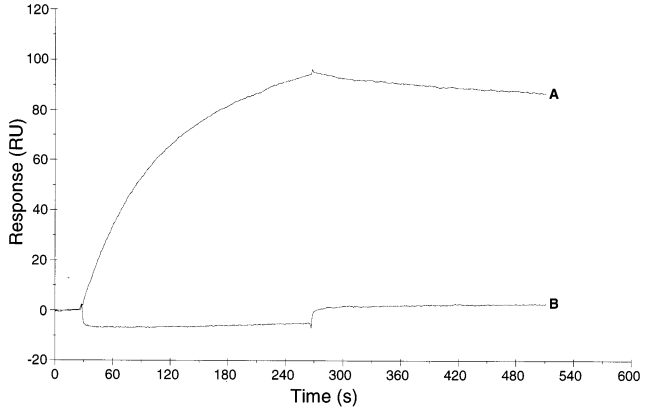

FIGURE 3: Specificity of the AMY2−BASI interaction determined by SPR. Curve A: interaction between AMY2 (155 nM) and immobilized BASI shown as RU monitored from 0 to 250 s for association and dissociation from 250 to 550 s. Curve B: lack of interaction for AMY1 (1166 nM). The measurements were carried out in 10 mM Hepes, 150 mM NaCl, pH 7.4, 0.005% P-20, and 1 mM $CaCl_2$ at 25 °C.

Binding Kinetics for BASI and AMY2 Sensor Chips. To determine the binding kinetics of the AMY2−BASI interaction, AMY2 was injected over immobilized BASI followed by buffer, and the reaction was measured in real time by recording the changes in surface plasmon resonance. The sensorgrams were analyzed and fitted to a single-site interaction model. The kinetic rate constants k_{on} and k_{off} were determined for several analyte concentrations in the range of 62−187 nM (Figure 2). The equilibrium dissociation constant (K_D) was calculated from the rate constants and found to be in the low nanomolar range. No binding of AMY1 to immobilized BASI was observed, demonstrating target enzyme specificity (Figure 3). Since similar binding kinetics was observed using either immobilized AMY2 or BASI, the data obtained validated the use of surface plasmon resonance for studying the AMY2−BASI binding (see Table 4 below). Equilibrium data were also analyzed by Scatchard analysis (not shown) (*37*) to give a K_D of 1.1 nM, in agreement with the value of 1.0 nM at pH 6.5 in 5 mM $CaCl_2$ (Table 1) calculated from the rate constants.

Table 1: Effect of Ca^{2+} Concentration on the AMY2−BASI Interaction Analyzed by Surface Plasmon Resonance at pH 5.5, 6.5, and 7.4[a]

$CaCl_2$ (mM)	$k_{on} \times 10^{+4}$ (M^{-1} s^{-1})	$k_{off} \times 10^{-4}$ (s^{-1})	K_D (nM)
pH 5.5			
$(2-6) \times 10^{-3}$	4.9(±0.7)	30.0(±4.3)	61.2(±12.4)
1	6.4(±0.3)	26.6(±0.2)	41.6(±2.0)
5	8.3(±1.0)	26.0(±0.6)	31.3(±3.8)
40	8.1(±0.4)	15.1(±0.3)	18.6(±1.0)
80	8.0(±0.5)	15.4(±0.5)	19.3(±1.4)
pH 6.5			
$(2-6) \times 10^{-3}$	6.2(±0.9)	18.5(±3.1)	29.8(±6.6)
0.1	11.0(±1.8)	7.2(±0.7)	6.5(±1.2)
1	16.4(±2.8)	4.1(±0.4)	2.5(±0.5)
5	20.0(±3.9)	1.9(±0.1)	1.0(±0.2)
20	18.0(±3.8)	2.0(±0.1)	1.1(±0.2)
pH 7.4			
$(2-6) \times 10^{-3}$	9.4(±0.7)	2.9(±0.1)	3.1(±0.3)
1	11.1(±0.4)	1.3(±0.2)	1.2(±0.2)
5	12.6(±3.1)	1.3(±0.07)	1.0(±0.3)
20	16.0(±2.6)	1.6(±0.2)	1.0(±0.2)
40	15.9(±2.1)	1.1(±0.1)	0.7(±0.1)
80	16.0(±2.2)	1.3(±0.1)	0.8(±0.1)

[a] The rate constants represent the mean of determinations using five AMY2 (analyte) concentrations from 20 to 200 nM. Standard deviations are shown in parentheses. Measurements were performed at 25 °C in 10 mM Mes, pH 5.5, 150 mM NaCl, and 0.005% P-20; 10 mM Mes, pH 6.5, and 0.005% P-20; or 10 mM Hepes, 150 mM NaCl, pH 7.4, and 0.005% P-20, at the $CaCl_2$ concentrations shown.

Ca^{2+}, Ionic Strength, and pH Dependence of BASI Binding to AMY2. The crystal structure of the AMY2−BASI complex contains a fully hydrated Ca^{2+} ion at the protein interface (Figure 1) that has been suggested to stabilize the complex (*13*). To understand its functional role, the Ca^{2+}-dependent binding of AMY2 to immobilized BASI was explored at pH 5.5, the optimum for starch-degrading activity of AMY2 (*38*) (Table 1). In the $[Ca^{2+}]$ range of 2×10^{-3} to 80 mM a modest but significant 3-fold increase in affinity of AMY2 for BASI occurred at pH 5.5 and $[Ca^{2+}] \geq 40$ mM. A 4-fold increase was determined at pH 7.4 where binding is also tighter, whereas at pH 6.5 a 30-fold improvement of the affinity occurred by increasing the $[Ca^{2+}]$ from the micromolar range to 5 mM (Table 1). The effect on the individual rate constants indicated that Ca^{2+} enhanced the binding of AMY2 to BASI mainly by reducing the rate of dissociation of the complex.

The AMY2 crystal structure contains three structural Ca^{2+} ions believed to be critical for the stability and activity of the enzyme (*15*, *39*, *40*). Indeed, no binding of AMY2 to immobilized BASI was detected in the presence of 3 mM EDTA at pH 7.4 (data not shown). A short injection of 50 mM EDTA in fact efficiently removed AMY2, hence regenerating the sensor chip surface (data not shown). When activity of AMY2 toward blue starch was assayed in the presence of 3 mM EDTA, it was reduced by 90% compared to conditions without EDTA (data not shown). These results support that the presence of free Ca^{2+} was essential for the AMY2 activity, and therefore discrimination by EDTA between the Ca^{2+} ions bound in the free enzyme and in the inhibitor complex was not possible.

General ionic strength dependence was determined at NaCl concentrations in the 0−1 M range (Table 2). The affinity was only less than 3-fold decreased at 1 M NaCl, as caused by small effects of both k_{on} and k_{off}, suggesting a minor role of long-range electrostatic forces for the association and dissociation kinetics.

Table 2: Ionic Strength Dependence of the Binding of AMY2 to Surface-Bound BASI at pH 6.5 and 8.0[a]

NaCl (mM)	$k_{on} \times 10^{+4}$ (M^{-1} s^{-1})	$k_{off} \times 10^{-4}$ (s^{-1})	K_D (nM)
pH 6.5			
0	18.3(±3.5)	2.0(±0.1)	1.1(±0.2)
150	13.5(±2.0)	2.6(±0.07)	1.9(±0.3)
300	13.8(±3.2)	2.9(±0.08)	2.1(±0.5)
500	11.9(±1.4)	3.1(±0.03)	2.6(±0.3)
1000	10.5(±1.2)	3.4(±0.02)	3.2(±0.4)
pH 8.0			
0	15.0(±2.6)	1.7(±0.1)	1.1(±0.2)
150	14.3(±3.0)	1.6(±0.2)	1.1(±0.3)
300	10.9(±1.2)	2.5(±0.4)	2.3(±0.4)
500	10.5(±1.6)	2.7(±0.1)	2.6(±0.4)
1000	8.5(±1.1)	3.1(±0.1)	3.6(±0.5)

[a] The rate constants represent the mean of determinations using five AMY2 (analyte) concentrations from 20 to 200 nM. Standard deviations are shown in parentheses. Measurements were performed at 25 °C in 10 mM Mes, pH 6.5, 5 mM $CaCl_2$, and 0.005% P-20 or 10 mM Hepes, pH 8.0, 5 mM $CaCl_2$, and 0.005% P-20, at the NaCl concentration shown.

Table 3: pH Dependence of the Binding of AMY2 to BASI[a]

pH	$k_{on} \times 10^{+4}$ (M^{-1} s^{-1})	$k_{off} \times 10^{-4}$ (s^{-1})	K_D (nM)
5.5	8.3(±1.0)	26.0(±0.6)	31.3(±3.8)
6.0	11.4(±2.6)	6.1(±0.3)	5.4(±1.2)
6.5	13.5(±2.0)	2.6(±0.07)	1.9(±0.3)
7.0	13.5(±2.6)	2.5(±0.08)	1.9(±0.4)
7.4	12.6(±3.1)	1.3(±0.07)	1.0(±0.3)
8.0	14.3(±3.0)	1.6(±0.2)	1.1(±0.3)

[a] The rate constants represent determinations using five AMY2 (analyte) concentrations from 20 to 200 nM. Standard deviations are shown in parentheses. Measurements were performed at 25 °C in 10 mM Hepes or 10 mM Mes, 0.15 M NaCl, 0.005% P-20, and 5 mM $CaCl_2$ at pH 8.0, 7.4, 7.0, 6.5, 6.0, and 5.5.

The pH dependence of the AMY2−BASI interaction was analyzed in the range from pH 5.5 to pH 8.0 (Table 3). The K_D was critically dependent on pH, and while k_{off} increased 20-fold upon lowering pH from 7.4 to 5.5, k_{on} did not change. The determined value for K_D of 31.3 nM at pH 5.5 was comparable with $K_D = 25.0$ nM at 27 °C obtained by ITC (see below).

Temperature Dependence of BASI Binding to AMY2. The binding kinetics of the AMY2−BASI complex was analyzed at five different temperatures from 5 to 40 °C with either BASI or AMY2 bound to the sensor chip (Table 4). The complex was slightly more stable at lower temperature as shown by the 3-fold lower K_D. The increase observed for K_D when the temperature was raised from 5 to 40 °C was due mainly to a 12-fold increase of k_{off}, k_{on} increasing only by 3−4-fold. These results showed that the K_D is weakly dependent on the temperature. The van't Hoff plot of the variation of K_D as a function of temperature (Figure 4) allowed calculation of the thermodynamic parameters at 25 °C, $\Delta H_{vH} = -25.2$ kJ mol^{-1} (BASI as ligand) and −34.0 kJ mol^{-1} (AMY2 as ligand) and $\Delta G° = -49.5$ kJ mol^{-1} (BASI as ligand) and −55.3 kJ mol^{-1} (AMY2 as ligand).

Isothermal Titration Calorimetry Analysis. The AMY2−BASI binding was characterized by a large exothermic heat ($\Delta H = -69 \pm 7$ kJ mol^{-1}) corresponding to a K_D of 25 nM

Table 4: Temperature Dependence of the AMY2−BASI Interaction Measured by SPR[a]

temp (°C)	$k_{on} \times 10^{+4}$ (M^{-1} s^{-1})	$k_{off} \times 10^{-4}$ (s^{-1})	K_D (nM)
BASI immobilized			
5	4.5(±0.2)	0.3(±0.1)	0.7(±0.2)
15	7.4(±0.6)	1.0(±0.6)	1.4(±0.8)
25	11.9(±1.6)	2.0(±0.1)	1.7(±0.2)
35	18.0(±3.5)	3.7(±0.5)	2.1(±0.5)
40	nd	nd	nd
AMY2 immobilized			
5	6.2(±2.6)	0.7(±0.5)	1.1(±0.9)
15	9.3(±4.6)	0.8(±0.5)	0.9(±0.7)
25	9.2(±3.2)	3.2(±0.05)	3.5(±1.2)
35	15.7(±3.6)	6.7(±1.4)	4.3(±1.3)
40	16.5(±4.7)	8.5(±1.4)	5.2(±1.7)

[a] Kinetic constants were obtained in 10 mM Hepes, pH 7.4, 0.15 M NaCl, 0.005% P-20, and 5 mM $CaCl_2$ at 5, 15, 25, 35, and 40 °C. Standard deviations are shown in parentheses. nd: not determined.

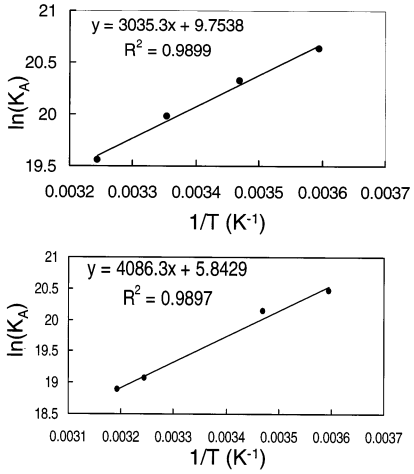

FIGURE 4: Linear van't Hoff plot of the AMY2−BASI interaction assuming a temperature-independent ΔH. Upper panel: BASI as ligand. Lower panel: AMY2 as ligand. $\Delta H°$ was determined from $\ln K = -\Delta H°/(RT) + \Delta S°/R$, $-\Delta H/R$ being the slope. $\Delta G°$ for the binding was calculated at 25 °C from $\Delta G° = -RT \ln K°$, where $R = 8.314$ J K^{-1} mol^{-1} is the gas constant and $K° = K_A C°$, where $C°$ is the concentration at the standard state (1 M) and $K_A = 1/K_D = k_{on}/k_{off}$.

Table 5: Temperature and pH Dependence of the AMY2−BASI Interaction Determined by ITC[a]

pH	temp (°C)	K_A (M^{-1})	$\Delta G°$ (kJ mol^{-1})	$\Delta H°$ (kJ mol^{-1})	$-T\Delta S°$ (kJ mol^{-1})
6.8	11	$(10 \pm 6) \times 10^7$	-44 ± 12	-60 ± 8	16 ± 15
	25	$(9 \pm 4) \times 10^7$	-45 ± 1	-98 ± 3	53 ± 3
	37	$(3 \pm 2) \times 10^7$	-49 ± 3	-86 ± 6	37 ± 7
	46	$(3 \pm 3) \times 10^7$	-46 ± 2	-94 ± 20	48 ± 20
	55	$(4 \pm 5) \times 10^7$	-47 ± 3	-100 ± 36	53 ± 35
5.5	27	$(4 \pm 2) \times 10^7$	-43.5 ± 12	-69 ± 7	26 ± 7

[a] Thermodynamic parameters were obtained from measurements in 40 mM Hepes, pH 6.8, 0.2 M NaCl, and 5 mM $CaCl_2$ or 40 mM sodium acetate, pH 5.5, and 5 mM $CaCl_2$.

(27 °C, pH 5.5) and an unfavorable change in entropy (Table 5) as shown using ITC. Figure 5 shows a representative thermogram and binding isotherm for the AMY2−BASI interaction. The calorimetric determination of K_D for the AMY2−BASI interaction was not reliable at higher pH (pH 8.0, 37 °C, not shown) due to too tight binding ($K_D \geq 10^9$ M^{-1}), and only the enthalpy and stoichiometry can be

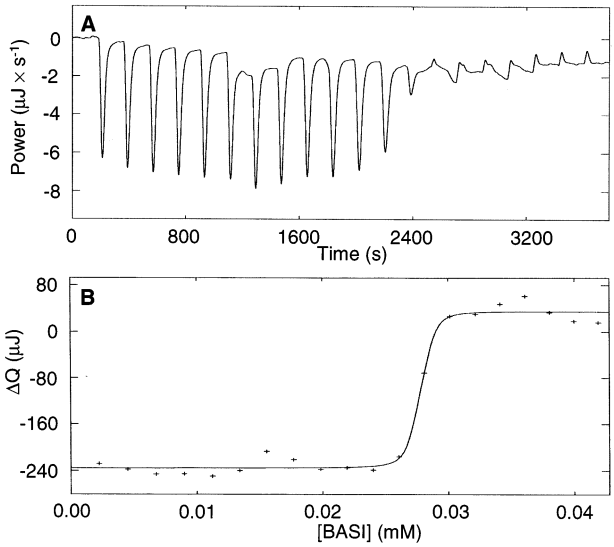

FIGURE 5: Thermogram and binding isotherm of the AMY2−BASI interaction. (A) Thermogram of AMY2 titrated with BASI at 11 °C in 40 mM Hepes, pH 6.8, 5 mM $CaCl_2$, and 0.2 M NaCl. (B) Binding isotherm shown in differential heat mode.

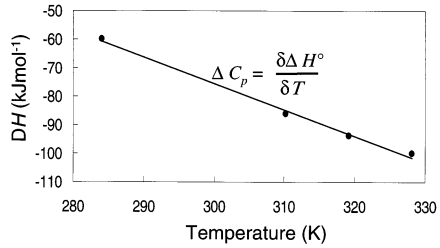

FIGURE 6: Heat capacity change for the AMY2−BASI interaction. Plot of data from ITC of the AMY2−BASI complex formation to give $\Delta C_p = -0.93$ kJ K^{-1} mol^{-1}. The correlation coefficient of the fit is 0.9948.

measured under these conditions (data not shown). The thermodynamic functions obtained by using ITC were remarkably temperature-insensitive in the interval from 25 to 55 °C, supporting that the hydrophobic effect was substantial. The binding reaction was characterized by a ΔC_p of −0.93 kJ K^{-1} mol^{-1} (Figure 6), which is comparable to typical values observed for protein−protein interactions ranging from −0.8 to −2.9 kJ K^{-1} mol^{-1} (*41*).

Conformational changes occurring during complex formation may be assessed from relationships that correlate structure with binding thermodynamics (*42*, *43*). By using an empirical equation developed by Xie and Freire (see Methods in ref *35*), the ΔC_p (−0.93 kJ K^{-1} mol^{-1}) and ΔH^{60} (−106 kJ cal mol^{-1}) values for the AMY2−BASI interaction infer that $\Delta ASA_{ap} = 1142$ Å^2 and $\Delta ASA_{pol} = 1117$ Å^2, yielding a total 2259 Å^2 surface area buried in the complex. This value is in excellent agreement with the 2355 Å^2 found for the AMY2−BASI interface in the crystal structure (*13*). The calculation thus supports that minimal structural change occurs in AMY2 or BASI during binding. While K_D showed only a 1.2-fold difference at pH 5.5 whether measured by ITC or SPR, the calorimetric enthalpy was much larger than the van't Hoff enthalpy determined from the SPR binding constants (Figure 4) or from the calorimetrically estimated binding contants. These van't Hoff enthalpies were in the range from −25 to −34.0 kJ mol^{-1} from linear van't Hoff

Table 6: SPR Analysis of the Temperature Dependence of the Interaction between Immobilized AMY2 and Mutants of BASI[a]

temp (°C)	$k_{on} \times 10^{+4}$ ($M^{-1} s^{-1}$)	$k_{off} \times 10^{-4}$ (s^{-1})	K_D (nM)
recombinant BASI			
5	7.6(±3.8)	1.3(±0.7)	1.7(±1.3)
15	11.2(±2.1)	2.2(±0.4)	2.0(±0.5)
25	16.0(±2.9)	2.8(±0.2)	1.8(±0.3)
35	21.0(±2.2)	6.8(±1.8)	3.2(±0.9)
40	20.2(±7.6)	9.2(±4.7)	4.6(±2.9)
K140L			
5	11.4(±7.2)	8.1(±1.3)	7.1(±4.6)
15	17.6(±7.1)	11.1(±0.9)	6.3(±2.6)
25	17.1(±3.1)	35.8(±1.7)	20.9(±3.9)
35	13.4(±5.7)	98.3(±67.5)	73.4(±59.3)
40	no binding detected		
E168Q			
5	6.2(±2.6)	1.9(±0.8)	3.1(±1.8)
15	13.4(±5.9)	3.1(±0.8)	2.3(±1.2)
25	14.5(±3.0)	12.6(±1.7)	8.7(±2.1)
35	31.4(±12.6)	19.7(±3.6)	6.3(±2.8)
40	36.1(±4.5)	18.3(±2.7)	5.1(±1.0)

[a] Kinetic constants were obtained in 10 mM Hepes, pH 7.4, 0.15 M NaCl, 0.005% P-20, and 5 mM $CaCl_2$ at 5, 15, 25, 35, and 40 °C. AMY2 was immobilized, while recombinant wild-type BASI and BASI mutants were analytes. Standard deviations are shown in parentheses.

plots or slightly more exothermic from nonlinear van't Hoff plots (not shown). In conclusion, the ITC experiment showed that BASI and AMY2 bind with favorable enthalpy, unfavorable entropy, and minimal structural changes.

Identification of BASI Hot Spots for Dissociation and Their Role in Thermal Stability of the AMY2−BASI Complex. The contributions of two charged BASI residues K140 and E168 to the electrostatic binding forces were probed by site-directed mutagenesis. In accordance with the weak salt dependence of k_{on}, substitution of a positively or negatively charged residue within the AMY2 inhibitory site of BASI (Figure 1) caused <1.5-fold variation of k_{on} for the K140L and E168Q mutants accompanied, however, by a 13- and 5-fold increase in k_{off}, respectively (Table 6), resulting in similar increases in K_D for the mutants. $\Delta\Delta G = \Delta G_{mutant} - \Delta G_{wild\ type}$ for K140L and E168Q was calculated at 25 °C to 6.1 and 3.9 kJ mol^{-1}, respectively. The result identifies these two BASI residues as hot spots for suppression of dissociation of the AMY2−BASI complex.

To further understand the effect on k_{on} and k_{off}, the temperature dependence of the AMY2 complex formation with the two BASI mutants was analyzed. Between 5 and 35 °C k_{on} increase <5-fold as compared to a 5-, 12-, and 10-fold increase of k_{off} for wild-type BASI and the K140L and the E168Q mutants, respectively (Table 6). Above 35 °C the K140L mutant was found to be unstable, and hence no binding to the immobilized AMY2 was detected. In contrast, k_{on} and k_{off} for E168Q BASI both increased 6−10-fold with increasing temperature from 5 to 40 °C, resulting in essentially unaffected K_D (Table 6). By comparison with recombinant wild-type BASI, where the rate constants increased 3−12-fold in the same temperature range (Tables 4 and 6), exchange of the positively charged K140 slightly weakened the complex and seemed to lead to destabilization of the BASI structure.

The structural integrity of the BASI mutants and effect on AMY2 binding were further evaluated by real-time binding kinetics to immobilized savinase, a subtilisin-type protease that does not share binding area with AMY2 (*17*). As the binding kinetics for savinase of the K140L and E168Q single mutants in the AMY2 binding site of BASI was essentially unchanged compared to BASI wild type, the observed effects on AMY2 binding (see above) were specific and not due to changes of the overall structure of BASI (Table 7).

Table 7: SPR Analysis of the Interaction between BASI Mutants or the AMY2−BASI Complex and Immobilized Savinase[a]

analyte	$k_{on} \times 10^{+4}$ ($M^{-1} s^{-1}$)	$k_{off} \times 10^{-4}$ (s^{-1})	K_D (nM)
BASI[b]	25.7(±4.5)	46.2(±1.8)	17.8(±3.2)
rBASI	20.2(±7.0)	41.8(±1.9)	20.7(±7.2)
K140L	26.7(±3.5)	49.9(±1.1)	18.7(±2.5)
E168Q	16.9(±1.4)	44.1(±3.5)	26.1(±3.0)
AMY2−BASI	14.7(±2.8)	40.3(±1.3)	27.4(±5.3)

[a] Kinetic constants were obtained in 10 mM Hepes, pH 7.4, 0.15 M NaCl, and 0.005% P-20 at 25 °C. Standard deviations are shown in parentheses. [b] BASI purified from barley seed.

The k_{off} for the interaction of the AMY2−BASI complex with savinase was similar to that of BASI, while the k_{on} for the complex was weakly reduced by 1.7-fold (Table 7). All together, these results identify savinase as a target protease for BASI (K_D = 17.8 nM) and indicate that α-amylase binding does not modulate and is independent of the interaction of BASI with protease.

DISCUSSION

Differences and Similarities to Other α-Amylase/α-Amylase Inhibitor Complexes. The presence of a fully hydrated Ca^{2+} at the center of the protein−protein interface in the AMY2−BASI complex, which is not observed in the structure of the free enzyme, makes AMY2−BASI unique among the known crystal structures of α-amylases in complex with proteinaceous inhibitors (*13*). Thus BASI does not bind directly to the three catalytic carboxyl groups in AMY2, but instead the Ca^{2+} via water molecules connects the three catalytic acids of AMY2 with side chains in BASI. In other types of α-amylase/protein inhibitor complexes the catalytic acids in the enzyme and the inhibitor directly interact (*18*−*20*), while in one case indirect interaction through a water molecule exists (*21*). BASI prevents substrate access to the active site by steric hindrance while substrate mimicry has been described for other α-amylase plant inhibitors (for review on α-amylase plant inhibitors, see ref *22*).

Kinetics and Energetics. A detailed analysis of the energetics and kinetics of the interactions between α-amylases and their proteinaceous inhibitors is required for better understanding of the molecular recognition principles and the mechanism of inhibition. Such insight will be helpful in the design of novel inhibitors and target enzyme variants. In the present work the binding kinetics and thermodynamics for the complex between AMY2 and BASI were described by using SPR and ITC.

The AMY2−BASI binding was in accordance with a simple 1:1 binding model when using either AMY2 or BASI immobilized on the sensor chip surface. The equilibrium binding constant (K_D = 1.1 nM at pH 8.0, 5 mM $CaCl_2$, 25 °C) for the complex was in agreement both with the

measurement of binding by ITC and with the inhibition constant (K_i = 0.22 nM) previously measured by AMY2 activity inhibition assays using insoluble blue starch as substrate (*44*). The high affinity of the AMY2−BASI complex was mainly due to a slow $k_{off} = 1.6 \times 10^{-4}$ s^{-1} (in 10 mM Hepes, pH 8.0, 5 mM $CaCl_2$, 25 °C), whereas $k_{on} = 14.3 \times 10^{+4}$ M^{-1} s^{-1} was in the range typical for protein−protein interactions of 10^5−10^6 M^{-1} s^{-1} (*45*−*47*). In comparison, interactions that are dominated by electrostatic steering can have k_{on} above 4×10^9 M^{-1} s^{-1}, while steric and orientation effects can reduce k_{on} to 10^3 M^{-1} s^{-1} (*45*, *48*−*50*). Moreover, the weak dependence of k_{on} on the ionic strength supported that long-range electrostatic attraction was not playing the major role in the AMY2−BASI formation. In agreement k_{on} was not significantly changed when a positively or negatively charged residue of BASI involved in the AMY2 binding site was exchanged by site-directed mutagenesis.

Since a previous stopped-flow fluorescence spectroscopy analysis of the AMY2−BASI complex formation (*14*) indicated a tight, fast two-state binding reaction, we also made the fitting of the present data using a two-state reaction mechanism involving a conformational change. However, as the closeness of this fit both by statistical analysis and by inspection of the binding curves was quite similar to one using the 1:1 Langmuir binding model, discrimination of the two models based on the SPR data alone was not possible. The kinetic rate constants calculated by the 1:1 binding model (see above) were fairly close to the reported k_{off} (0.7×10^{-4} s^{-1}) (*14*) obtained by stopped-flow fluorescence spectroscopy analysis, while a 6-fold difference was found for k_{on} ($82 \times 10^{+4}$ M^{-1} s^{-1}) (*14*). The reason for the lower value of k_{on} measured by SPR is unclear, but it may stem from effects of chip surface heterogeneity and reduced diffusion rate within the dextran hydrogel matrix (*51*, *52*).

pH Dependence and Hot Spots. The binding affinity was increased 17-fold by increasing the pH from 5.5 to 7, which was comparable with the 7-fold increase reported previously using fluorescence titration to monitor the impact of pH on complex formation (*53*). This clear dependence of k_{off} on pH may be explained by titration of carboxyl groups and histidine residues at the protein interface which had somewhat elevated and reduced pK_a values, respectively. Among the contacts reported for the AMY2−BASI complex there are eight carboxyl groups, $Asp150_{BASI}$, $Glu168_{BASI}$, $Asp138_{AMY2}$, $Asp142_{AMY2}$, $Glu129_{BASI}$, $Glu204_{AMY2}$, $Asp179_{AMY2}$, and $Asp289_{AMY2}$, of which the four latter are water-mediated contacts, and two histidine residues $His295_{AMY2}$ and $His29_{BASI}$ (*13*). The Glu168 was selected for mutational analysis. This residue forms both a salt bridge to $Lys182_{AMY2}$ and a hydrogen bond to one of the Ca^{2+}-coordinated water molecules (Figure 1). Weakened Ca^{2+} dependence compared to wild-type BASI (see below) was observed for E168Q BASI, which indirectly supports the fully hydrated Ca^{2+} at the protein interface to play a critical role (B. C. Bønsager, P. K. Nielsen, M. Prætorius-Ibba, and B. Svensson, unpublished data).

Electrostatic Screening. Another changed key residue Lys140 from one of the β-strands of BASI forms a salt bridge to Asp142 in domain B of AMY2 (Figure 1). Substitution of Glu168 with Gln and Lys140 with Leu resulted in 5- and 12-fold decreases, respectively, of the affinity essentially due to the increase of k_{off}. The identification of these two charged residues as hot spots was in accordance with a dominant role of short-range electrostatic forces for the dissociation step as shown by pH dependence and thermal stability of the AMY2−BASI complex. k_{off}, however, was independent of the salt concentration, suggesting that global or long-range electrostatic forces do not play a critical role in the AMY2−BASI dissociation (*54*). The lack of effect on the short-range electrostatic forces by screening with 1 M NaCl showed that the salt bridges are likely to be shielded in the formed complex. Interestingly, removal of a positive charge in K140L reduced the thermal stability of the complex significantly, while increasing the positive charge of BASI by the removal of a negative charge had no effect on the stability. Negative charged residues close to K140 in BASI include E128 and D150. Thus repulsive electrostatic forces between those negative surface charges may destabilize BASI.

Thermodynamics. The formation of the complex between AMY2 and BASI resulted in an entropy penalty that in addition to the losses in translational and rotational freedom may be explained by ordering of AMY2 interfacial residues upon binding since comparison of the temperature factor between the free and bound AMY2 crystal structure decreased for most interfacial residues (*13*). The *B*-factors of the residues in free BASI, however, are unknown and must await structure determination of free BASI. Capturing a Ca^{2+} ion and its hydrating water molecules also carries a significant entropy penalty. This apparently overcomes the entropy of solvent rearrangement due to binding. The heat capacity change, ΔC_p, for the binding reaction was small, which is typical for protein−protein interactions that do not involve a large conformational change (*35*). In accordance, the calculated accessible surface area from the thermodynamic data indicated that only minimal structural changes were likely to take place in AMY2 or BASI in the complex.

Comparison of Equilibrium and Thermodynamic Constants Determined by SPR and ITC. While the K_D values for AMY2−BASI measured by SPR correlated well with the values acquired by ITC, the calorimetric enthalpy was much larger than the van't Hoff enthalpy. However, discrepancies between van't Hoff and calorimetric enthalpies have been frequently observed and may be due to several different reasons (*55*−*58*). These reasons include erroneous concentration of the ligand (resulting in wrong stoichiometry and wrong estimation of ΔH), poor experimental design (resulting in large statistically correlated errors), regression analysis of the binding isotherm using equations referring to a wrong mechanism, and ignoring possible heat effects from changes in protonization states associated with the binding. Errors may occur in the determination of binding constants or enthalpies or both. In our case, we observe reasonably consistent binding constants obtained from calorimetry and SPR, so the error most likely lies in the enthalpy measurements. We feel confident that the determinations of protein concentrations and the experimental protocol for the ITC measurements are of good standard. The simplest possible binding mechanism was used in the analysis of the binding isotherms, and good fits were obtained. However, this does not exclude that a more complicated binding mechanism may be the correct one, but which leads to binding isotherms that

mathematically can be described by equations derived from a simpler mechanism. It is difficult to design experiments that could test this problem. The most likely source of the observed discrepancy in the present case is changes in protonization. Since the titrations were only conducted in one buffer system (Hepes), it cannot be decided whether there is a change in protonization. Hepes has a heat of proton association of −20.01 kJ mol^{-1}. Since the discrepancy amounts to approximately 55−90 kJ mol^{-1}, more exothermic enthalpies in ITC are obtained compared to SPR depending on the conditions. This would correspond to a release of approximately 3−4 protons from the proteins upon binding, which seems to be an entirely realistic number from a protein−protein interaction. Importantly, use of ITC allows determination of enthalpy independent of the binding reaction model and is the preferred method for defining thermodynamic reaction parameters (*60*). Measurement of K_D is generally method dependent (59). Thus the small difference (1.2−5-fold) found for K_D whether determined by SPR or ITC may due to the difference in experimental conditions associated with each measurement. SPR is a surface-based technique that involves immobilization of one of the binding partners, i.e., it is a two-phase measurement, while ITC is a solution-phase technique where high protein concentrations and reduced pH were required to determine K_D.

The Interface Ca^{2+}. The crystal structure of AMY2−BASI suggests that the fully hydrated Ca^{2+} contributes electrostatic stabilization of the complex (*13*). In accordance at pH 6.5 the affinity was increased 30-fold by adding Ca^{2+} to 5 mM. One may speculate that the 31-fold higher K_D at pH 5.5 compared to K_D at pH 6.5 reflects weaker binding because a deprotonated carboxyl and histidine are important. At pH 6.5 the electrostatic binding involving carboxylate reduces the K_D but the protonated imidazole group counteracts binding, whereas finally at pH 7.4 this repulsion is eliminated by deprotonation of the histidine side chain. Possible candidate residues are $His29_{BASI}$ and $His295_{AMY2}$ (*13*). In reality, however, the mechanism of this increase remains unclear also because of the lack of possibility in discriminating in such experiments between Ca^{2+} effects at the level of the three structural Ca^{2+} ions in AMY2 and the fully hydrated fourth Ca^{2+} at the AMY2−BASI interface.

Conclusion. SPR studies were used to demonstrate a critical role of Ca^{2+} in modulating AMY2−BASI dissociation. Calculations based on thermodynamic data obtained by ITC indicated that the complex formation only involves minimal structural changes. The importance of electrostatic forces for complex formation was demonstrated by identification of hot spots for dissociation and pH dependence. However, electrostatic screening by salt was not achieved, suggesting a minor role for long-range electrostatic forces in both the binding and dissociation steps and the presence of stronger short-range electrostatic interactions in the formed complex. The same principles for electrostatic forces have also been reported for an unrelated protein−protein interaction between an enzyme and its protein inhibitor (*54*). Finally, the work allowed direct comparison of two biophysical techniques and provides for the first time evidence that suggests an important role of Ca^{2+} in the regulation of the interaction between an α-amylase and its proteinaceous inhibitor in vivo.

ACKNOWLEDGMENT

Sidsel Ehlers is gratefully acknowledged for technical assistance with the preparation of AMY2-2 and BASI, Dr. Mette Prætorius-Ibba is thanked for the BASI intein expression plasmid, and Dr. Klaus Breddam is thanked for advice on savinase.

REFERENCES

1. Mundy, J., Svendsen, I., and Hejgaard, J. (1983) *Carlsberg Res. Commun. 48*, 81−91.
2. Abe, J., Sidenius, U., and Svensson, B. (1993) *Biochem. J. 293*, 151−155.
3. Weselake, R. J., MacGregor, A. W., and Hill, R. D. (1983) *Plant Physiol. 72*, 809−812.
4. Rogers, J. C., and Milliman, C. (1983) *J. Biol. Chem. 258*, 8169−8174.
5. Rogers, J. C. (1985) *J. Biol. Chem. 260*, 3731−3738.
6. Svensson, B., Mundy, J., Gibson, R. M., and Svendsen, I. (1985) *Carlsberg Res. Commun. 50*, 15−22.
7. Zemke, K. J., Müller-Fahrnow, A., Jany, K. D., Pal, G. P., and Saenger, W. (1991) *FEBS Lett. 279*, 240−242.
8. Mundy, J., Svendsen, I., and Hejgaard, J. (1984) *FEBS Lett. 167*, 210−214.
9. Ohtsubo, K., and Richardson, M. (1992) *FEBS Lett. 309*, 68−72.
10. Swindells, M. B., and Thornton, J. M. (1993) *Protein Eng. 6*, 711−715.
11. Liu, C., Gaspar, J. A., Wong, H. J., and Meiering, E. M. (2002) *Protein Sci. 11*, 669−679.
12. Zhu, X., Komiya, H., Chirino, A., Faham, S., Fox, G. M., Arakawa, T., Hsu, B. T., and Ress, D. C. (1991) *Science 251*, 90−93.
13. Vallée, F., Kadziola, A., Bourne, Y., Juy, M., Rodenburg, K. W., Svensson, B., and Haser, R. (1998) *Structure 6*, 649−659.
14. Sidenius, U., Olsen, K., Svensson, B., and Christensen, U. (1995) *FEBS Lett. 361*, 250−254.
15. Kadziola, A., Abe, J., Svensson, B., and Haser, R. (1994) *J. Mol. Biol. 239*, 104−121.
16. Kadziola, A., Søgaard, M., Svensson, B., and Haser, R. (1998) *J. Mol. Biol. 278*, 205−217.
17. Pal, G. P., Kavounis, C. A., Jany, K. D., and Tsernoglou, D. (1994) *FEBS Lett. 341*, 167−170.
18. Wiegand, G., Epp, O., and Huber, R. (1995) *J. Mol. Biol. 247*, 99−110.
19. Bompard-Gilles, C., Rousseau, P., Rouge, P., and Payan, F. (1996) *Structure 15*, 1441−1452.
20. Strobl, S., Maskos, K., Wiegand, G., Huber, R., Gomis-Ruth, F. X., and Glockshuber, R.(1998) *Structure 6*, 911−921.
21. Pereira, P. J., Lozanov, V., Patthy, A., Huber, R., Bode, W., Pongor, S., and Strobl, S. (1999) *Struct. Folding Des. 7*, 1079−1088.
22. Franco, O. L., Rigden, D. J., Melo, F. R., and Grossi-De-Sa, M. F. (2002) *Eur. J. Biochem. 269*, 397−412.
23. Ajandouz, E. H., Abe, J., Svensson, B., and Marchis-Mouren, G. (1992) *Biochim. Biophys. Acta 1159*, 193−202.
24. Gibson, R. M., and Svensson, B. (1986) *Carlsberg Res. Commun. 51*, 295−308.
25. Svendsen, I., Hejgaard, J., and Mundy, J. (1986) *Carlsberg Res. Commun. 51*, 43−50.
26. Grøn, H., Bech, L. M., Branner, S., and Breddam, K. (1990) *Eur. J. Biochem. 194*, 897−901.
27. Leah, R., and Mundy, J. (1989) *Plant Mol. Biol. 12*, 673−682.
28. Chong, S., Mersha, F. B., Comb, D. G., Scott, M. E., Landry, D., Vence, L. M., Perler, F. B., Benner, J., Kucera, R. B., Hirvonen, C. A., Pelletier, J. J., Paulus, H., Xu, M.-Q. (1997) *Gene 192*, 277−281.
29. Matsui, I., and Svensson, B. (1997) *J. Biol. Chem. 272*, 22456−22463.
30. Karlsson, R., and Fält, A. (1997) *J. Immunol. Methods 200*, 121−133.
31. Myszka, D. G. (2000) *Methods Enzymol. 323*, 325−340.
32. Schuck, P. (1997) *Annu. Rev. Biophys. Biomol. Struct. 26*, 541−566.
33. Karlsson, R., Michaelsson, A., and Mattsson, L. (1991) *J. Immunol. Methods 145*, 229−240.
34. Wiseman, T., Williston, S., Brandts, J. F., and Lin, L. N. (1989) *Anal. Biochem. 179*, 131−137.

35. Xie, D., and Freire, E. (1994) *Proteins 19*, 291−301.
36. Berman, H. M., Westbrook, J., Feng, Z., Gilliland, G., Bhat, T. N., Weissig, H., Shindyalov, I. N., and Bourne, P. E. (2000) *Nucleic Acids Res. 28*, 235−242.
37. De Crescenzo, G., Grothe, S., Lortie, R., Debanne, M. T., and O'Connor-McCourt, M. (2000) *Biochemistry 39*, 9466−9476.
38. Søgaard, M., and Svensson, B. (1990) Gene *94*, 173−179.
39. Bush, D. S., Sticher, L., van Huystee, R., Wagner, D., and Jones, R. L. (1989) *J. Biol. Chem. 264*, 19392−19398.
40. Bertoft, E., Andtfolk, C., and Kulp S.-E. (1984) *J. Inst. Brew. 90*, 298−302.
41. Stites, W. E. (1997) *Chem. Rev. 97*, 1233−1250.
42. Spolar, R. S., and Record, M. T., Jr. (1994) *Science 263*, 777−784.
43. Freire, E. (1995) *Annu. Rev. Biophys. Biomol. Struct. 24*, 141−165.
44. Rodenburg, K., Vallée, F., Juge, N., Aghajari, N., Guo, X., Haser, R., and Svensson, B. (2000) *Eur. J. Biochem. 267*, 1019−1029.
45. Doyle, M. L., Brigham-Burke, M., Blackburn, M. N., Brooks, I. S., Smith, T. M., Newman, R., Reff, M., Stafford, W. F., III, Sweet, R. W., Truneh, A., Hensley P., and O'Shannessy, D. J. (2000) *Methods Enzymol. 323*, 207−230.
46. Koren, R., and Hammes, G. G. (1976) *Biochemistry 15*, 1165−1171.
47. Northrup, S. H., and Erickson, H. P. (1992) *Proc. Natl. Acad. Sci. U.S.A. 89*, 3338−3342.
48. Wallis, R., Moore, G. R., James, R., and Kleanthous, C. (1995) *Biochemistry 34*, 13743−13750.
49. Pontius, B. W. (1993) *Trends Biochem. Sci. 18*, 181−186.
50. Raman, C. S., Jemmerson, R., Nall, B. T., and Allen, M. J. (1992) *Biochemistry 31*, 10370−10379.
51. Quinn, J. G., and O'Kennedy, R. (2001) *Anal. Biochem. 290*, 36−46.
52. O'Shannessy, D. J., and Winzor, D. J. (1996) *Anal. Biochem. 236*, 275−283.
53. Halayko, A. J., Hill, R. D., and Svensson, B. (1986) *Biochim. Biophys. Acta 873*, 92−101.
54. Selzer, T., Albeck, S., and Schreiber, G. (2000) *Nat. Struct. Biol. 7*, 537−541.
55. Naghibi, H., Tamura, A., and Sturtevant, J. M. (1995) *Proc. Natl. Acad. Sci. U.S.A. 92*, 5597−5599.
56. Chaires, J. B. (1997) *Biophys. Chem. 64*, 15−23.
57. Sinha, A., Yadav, S., Ahmad, R., and Ahmad, F. (2000) *Biochem. J. 345*, 711−717.
58. Horn, J. R., Russell, D., Lewis, E. A., and Murphy, K. P. (2001) *Biochemistry 40*, 1774−1778.
59. Connors, K. A (1987) in *Binding Constants. The Measurement of Molecular Complex Stability*, pp 363−372, John Wiley & Sons, New York.
60. Hensley, P., Doyle, M. L., Myszka, D. G., Woody, R. W., Brigham-Burke, M. R., Erickson-Miller, C. L., Griffin, C. A., Jones, C. S., McNulty, D. E., O'Brien, S. P., Amegadzie, B. Y., MacKenzie, L., Ryan, M. D., and Young, P. R. (2000) *Methods Enzymol. 323*, 177−207.

BI020508+